Nanoscale Horizons

ROYAL SOCIETY OF CHEMISTRY

REVIEW

View Article Online
View Journal

Cite this: DOI: 10.1039/d5nh00621j

Impact of exposure conditions on the uptake of nanoparticles by cultured cells

Yalan Huang, †[abc] Xing Sun,†[b] Sabine Vidal-Y-Sy,[d] Yuanyuan Wang,[d] Miao Feng,[b] Ziyao Liu,[b] Yang Liu,[b] Bing Qi,[b] Yanan Kang,[b] Christian Gorzelanny,[d] Wolfgang J. Parak *[b] and Neus Feliu *[be]

The way in which nanoparticles interact with cells in basic cell culture models depends not only on the physicochemical properties of the nanoparticles and the biological properties of different cell types but also on the geometry used for the cell culture. In this study, the effect of cell culture geometry on the uptake of nanoparticles is compared quantitatively. HeLa cells are used for the entire study in order to minimize cell-specific effects. Polymer-coated gold nanoparticles with similar surface chemistry, but different sizes, C are used as the model system. Four different cell culture geometries were investigated: adherent cells with static medium above them, adherent cells with medium flowing above them in a microfluidics channel, adherent cells where the cell culture is slowly rotated, and suspended cells in a rotating culture. The size-dependent uptake of the different nanoparticles by the cells under these culture conditions is analyzed in terms of elemental intracellular gold per cell. The results show that relating the uptake of nanoparticles to their physicochemical properties may depend on the applied cell culture geometry. While adherent cells in the static culture favor uptake of larger nanoparticles, suspended cells in rotation culture preferentially take up smaller nanoparticles. Direct comparison of the uptake of six different nanoparticle types in cells in four different cell culture geometries enables quantitative analysis. This study suggests that the geometry of *in vitro* cell culture systems should be optimized with respect to the *in vivo* scenarios they emulate. While this fact is known and has been discussed by several groups, in this work, the effects can be quantitatively discussed, thanks to a systematic direct comparison.

Received 4th September 2025,
Accepted 6th November 2025

DOI: 10.1039/d5nh00621j

rsc.li/nanoscale-horizons

Introduction

For the development of potential nanomedicines, it is very important to understand the uptake of nanoparticles (NPs) by cells. It would be very beneficial to correlate the uptake of NPs by cells with their physicochemical properties, enabling the NPs to be tailored to the requirements of their specific applications.[1] Ultimately, nanomedicine deals with the *in vivo* administration of NPs and thus cellular uptake needs to be investigated *in vivo*. However, ethical, economical and technical constraints—such as the complexity of *in vivo* NP–cell interactions—limit animal use, highlighting the value of *in vitro* studies. These studies aid in elucidating basic mechanisms and serve as a prescreening tool, reducing the number of animals required for *in vivo* experiments.

In vitro studies comprise many levels of complexity, starting from adherent static two-dimensional cell cultures to three-dimensional organoid and tissue models.[2–6] Again, for such *in vitro* systems, complexity can also blur the observation of fundamental principles of NP–cell interaction. On the one hand, simpler, more idealized model systems allow basic mechanisms to be more clearly unraveled. On the other hand, oversimplified systems may not reflect what is actually happening in the "real" system. The challenge thus is to understand the limitations of model systems, and thus choose appropriate model systems to address the biological question to be investigated.

Even for simple cell cultures comprising only one type of cell, the influence of the culture conditions on the cellular uptake of NPs is known. Different cell culture conditions—such as static (fluid), suspension, and dynamic (*e.g.*, shear stress or perfusion)—are crucial for studying cellular uptake, because they simulate diverse physiological environments and

[a] *Department of Ultrasound, Shenzhen People's Hospital (The First Affiliated Hospital, Southern University of Science and Technology; The Second Clinical Medical College, Jinan University), Shenzhen 518020, China*
[b] *Center for Hybrid Nanostructures (CHyN), Universität Hamburg, 22607 Hamburg, Germany. E-mail: wolfgang.parak@uni-hamburg.de, neus.feliu@physnet.uni-hamburg.de*
[c] *Post-doctoral Scientific Research Station of Basic Medicine, Jinan University, Guangzhou 510632, China*
[d] *Department of Dermatology, University Medical Center Hamburg-Eppendorf, 20251 Hamburg, Germany*
[e] *Fraunhofer Center for Applied Nanotechnology (CAN), 20146 Hamburg, Germany*
† Equal contribution.

significantly influence cell behavior.[7–10] These conditions affect morphology, receptor expression, endocytosis mechanisms, and interactions with nanoparticles (NPs), drugs, or other cells, all of which impact uptake efficiency.[11–14] Xia *et al.*[15] compared upright and inverted cell cultures and found that the uptake of Au NPs was affected by their sedimentation and diffusion rates, and was independent of their size, shape, density, surface modification, and initial concentration. Han *et al.*[16] investigated how acute and chronic shear stress differentially regulate the endothelial uptake of nanocarriers targeting PECAM-1. They found that chronic shear stress inhibits endocytosis through the formation of actin stress fibers, while acute shear stress enhances uptake *via* PECAM-mediated signaling pathways. Hammond *et al.*[17] developed a novel and cost-effective suspension culture device, the cell spinpod, designed to apply physiologically relevant fluid shear stress to renal proximal tubular cells. Beresova *et al.*[18] developed a novel shear stress generator that mimics disturbed fluid flow conditions to study cellular responses under physiologically relevant mechanical stress.

As can be seen from this summary, different cell culture conditions may, on the one hand, affect the behavior of the cells, as they may change the way NPs interact with cells. On the other hand, they also influence the way the NPs come into contact with the cells. This is a step dominated by physical effects, such as sedimentation due to gravity[19,20] or flow. Once the NPs have come into contact with cells, the biological process of endocytosis begins. In this work, we want to focus on the physical effects of different cell culture systems, disregarding the biological variety of different cells. For this reason, all experiments were performed with the same cell system: human cervical adenocarcinoma cells (HeLa cell line CCL2), a standard system used in many uptake studies of NPs. Four different exposure geometries were compared: adherent 2D static culture, adherent culture under flow, adherent culture under rotation, and suspension culture under rotation; see Fig. 1.

Materials and methods

The materials and methods used in this paper follow previously published protocols.[19,21] Spherical Au NPs of 4 different designated core diameters (5 nm, 25 nm, 50 nm, 100 nm) and Au nanorods (NRs) of 2 different lengths (40 nm, 100 nm) were synthesized in aqueous solution, transferred to the organic phase, and re-solubilized by coating with poly(isobutylene-*alt*-maleic anhydride)-*graft*-dodecylamine (PMA).[21,22] Standard physicochemical characterization methods, such as transmission electron microscopy (TEM) and dynamic light scattering (DLS), were employed.[21] HeLa cells in different cell culture geometries (see Fig. 1) were exposed for t_{exp} = 4 h, 8 h, and 24 h to the Au NPs at a concentration of $C_{Au(UV)}$ = 20 μg mL^{-1}, referring to the mass concentration of elemental gold, in serum-supplemented medium (see (SI) for details). After this, the amount of elemental gold per cell ($m_{Au/cell}$) was determined using inductively coupled plasma mass spectrometry (ICP–MS).

Results and discussion

Nanoparticle synthesis and characterization

The synthesis of the Au NPs followed standard protocols.[19,21] Physicochemical characterization of the NPs indicated the successful reproduction of these protocols. Notably, due to the large quantity of Au NPs needed to quantify the uptake of Au NP by cells, for each NP type, several batches following the

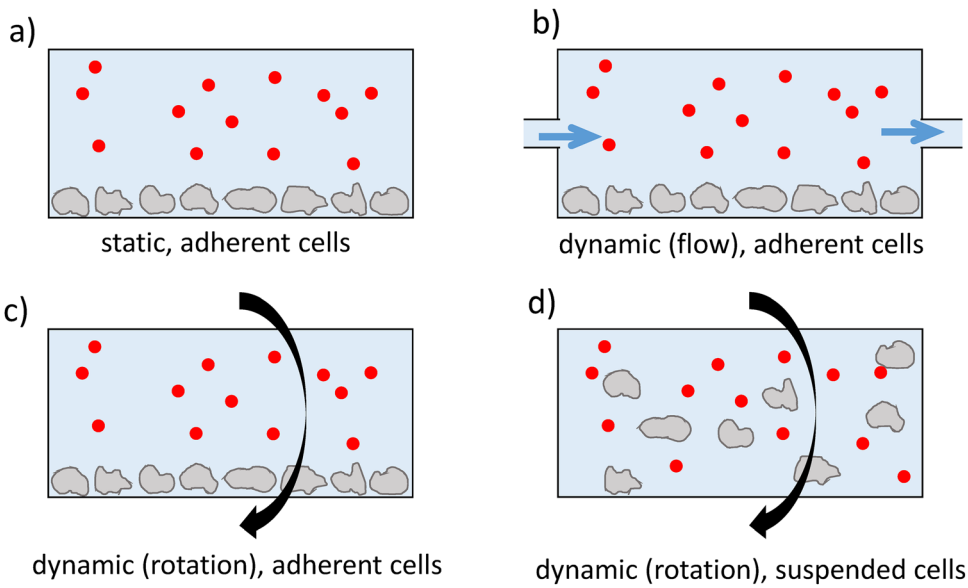

Fig. 1 Comparison of the different cell culture geometries used in this study. The cells are drawn in grey and the NPs in red. (a) Adherent cells under static incubation conditions, (b) adherent cells under dynamic incubation conditions, *i.e.* under flow, (c) adherent cells under dynamic incubation conditions, *i.e.* under rotation of the culture flask, (d) suspended cells under dynamic incubation conditions, *i.e.* under rotation of the culture flask.

Table 1 Basic characterization data for the different NP/NR samples: core diameter, as determined by TEM d_c; core length for the NRs, as determined by TEM L_c; mean hydrodynamic diameter, as determined from the DLS number distribution $d_{h(N)}$ and zeta potential ζ, both recorded in water. Data are given as mean value ± standard deviation (SD). Additional characterization data are included in Table SI-4

Sample	d_c [nm]	L_c [nm]	$d_{h(N)}$ [nm]	ζ [mV]
5 nm Au NPs	4.8 ± 0.9	—	15.5 ± 0.3	−31.8 ± 2.3
25 nm Au NPs	25.8 ± 1.3	—	30.6 ± 3.5	−40.6 ± 1.9
50 nm Au NPs	50.4 ± 4.9	—	47.9 ± 2.2	−38.9 ± 0.9
100 nm Au NPs	101.0 ± 7.8	—	109.4 ± 8.7	−47.1 ± 2.1
40 nm Au NRs	15.7 ± 1.9	39.3 ± 2.5	—	−39.1 ± 2.1
100 nm Au NRs	25.2 ± 1.4	99.3 ± 3.9	—	−41.0 ± 3.0

same protocol were produced and used; the physicochemical characterization reported here was not undertaken separately for each individual batch but represents data from one batch from each NP type. This is assumed to be justifiable, as the synthesis protocols are highly reproducible and thus batch-to-batch variations are considered irrelevant for the present study.

The different sizes and shapes of the 6 different NP types were verified with transmission electron microscopy (Fig. SI-1) and from the images the mean NP core (*i.e.* the Au part) diameters (d_c) and, in the case of the rod shaped NPs (NRs), the mean lengths (L_c) were also determined (Table 1 and Fig. SI-2). Based on this, the volumes of the NPs and NRs were calculated using the idealized geometry of spheres and cylinders, and, by using the density of bulk gold, the molar mass of each of the different NP types was estimated (Table SI-1). By measuring the elemental amount of gold in an NP solution by inductively coupled plasma mass spectrometry (ICP–MS), the mass concentration of the NPs $C_{Au(ICP)}$ [μg L^{-1}] could be determined. Alternatively, the molar concentration of Au NPs $c_{NP(UV)}$ [nM] was determined by measuring the absorption at 450 nm and using the Lambert–Beer law with extinction coefficients taken from the literature (Table SI-2).[23] By using the estimated molar mass of the NPs, the molar concentration could be converted into a mass concentration, $C_{Au(UV)}$ [μg L^{-1}]. We note that the determination of the concentration of Au NPs is affected by errors[24] (here, in particular, the assumption of perfect geometries of spheres/cylinders and extremely narrow size distribution) and thus $C_{Au(ICP)}$ and $C_{Au(UV)}$ are also not identical (Tables SI-2 and SI-3). The error in concentration determination needs to be considered when interpreting the results for the uptake of NP by cells.

All NPs were coated with the same amphiphilic polymer (PMA). Thus, their surface chemistry should be as similar as possible. This can be seen in the zeta potentials all being highly negative (Table 1 and Fig. SI-4) and in the comparable dynamic interfacial tension of the NP solutions (Fig. SI-6).[25] In water, apart from the 5 nm Au NPs where some small aggregates cannot be excluded, the hydrodynamic diameters are comparable to the core diameters (and there is also the several nm thick polymer shell[26]) (Table 1 and Fig. SI-3), as the surface plasmon peaks are clearly visible (Fig. SI-5), demonstrating colloidal stability. We note that, while the big NPs (in particular the 100 nm Au NPs) are not agglomerated and are well dispersed (which is why they are termed colloidally stable), there will be sedimentation effects due to gravity.[19,20]

Cell culture and exposure conditions in 4 different geometries and protocols to quantify the amount of internalized NPs

Culturing of HeLa cells was performed in the 4 geometries depicted in Fig. 1 (and Fig. SII-1 and Fig. SII-2). The culture geometry had an effect on proliferation, where the suspended cells grew much more slowly than the adherent cells (Fig. SII-3). For the experiments into NP uptake by cells, maintenance of cell viability under the used exposure geometries and conditions of $C_{Au(UV)}$ = 20 μg mL^{-1} was ensured (Fig. SIII-1 to Fig. SIII-4).

For the uptake studies, the 4 geometries depicted in Fig. 1 were used, while some of the exposure parameters were varied: in particular, the exposure concentration $C_{Au(UV)}$ = 10 μg mL^{-1} and 20 μg mL^{-1}, the exposure time t_{ext} = 4 h, 8 h, and 24 h, and the volume V_{exp} = 3 mL and 6 mL of the cell culture medium used in each flask (apart from the flow channel geometry, where only 6 mL was used). After exposure of the cells in serum-supplemented medium to the NPs for a time of t_{ext}, in the case of adherent cells, the cells were detached from the culture dish by trypsinization. In all cases, the cells were then pelleted by centrifugation. Following the washing steps, the number of cells was counted with a counting chamber under an optical microscope. The mass of elemental gold in the cells was determined by ICP–MS, leading to the amount of gold per cell $m_{Au/cell}$. Considering this methodology, the following points need to be mentioned. First, ICP–MS also records NPs merely adhering to the cell surface, which have not been endocytosed, and may remain despite the washing steps. There are ways to completely remove such adherent NPs: for example, by etching or other techniques.[27,28] However, this was not carried out here, as the number of adherent NPs after washing was considered minor compared to the actually endocytosed NPs. For a discussion on distinguishing between adherent and endocytosed NPs, we refer to another study.[29] Second, as mentioned, UV-vis absorption spectroscopy and ICP–MS give different NP concentration results. Ideally, the same method should be used to determine the concentration of the NP in the exposure solution, C_{Au}, and the gold content in cells, $m_{Au/cell}$. However, for convenience, in the present study, the exposure concentration $C_{Au(UV)}$ was determined by UV/vis absorption spectroscopy, while the NP quantification in cells $m_{Au/cell}$ was done with ICP–MS, and a correction was applied so that both determination of NP exposure concentration and quantification of internalized NPs followed the same metrics (see Table SIV-9). Thus, the final data directly relate the intracellular Au amount to the Au dose the cells were exposed to.

A summary of the NP uptake results is presented in Fig. 2 (the whole set of uptake data is provided in Fig. SIV-1 to SIV-10 and Tables SIV-1 to SIV-4). In all exposure geometries, there is a time (t_{exp})-dependent uptake of NPs (Fig. SIV-2, SIV-4, SIV-6 and SIV-10), as known from previous studies.[21,30] Uptake of NPs is also concentration ($C_{Au(UV)}$) dependent (Fig. SIV-1, SIV-3, SIV-5 and SIV-9), again in agreement with typical findings in the literature.[21,30] The NP uptake was not influenced by the volume

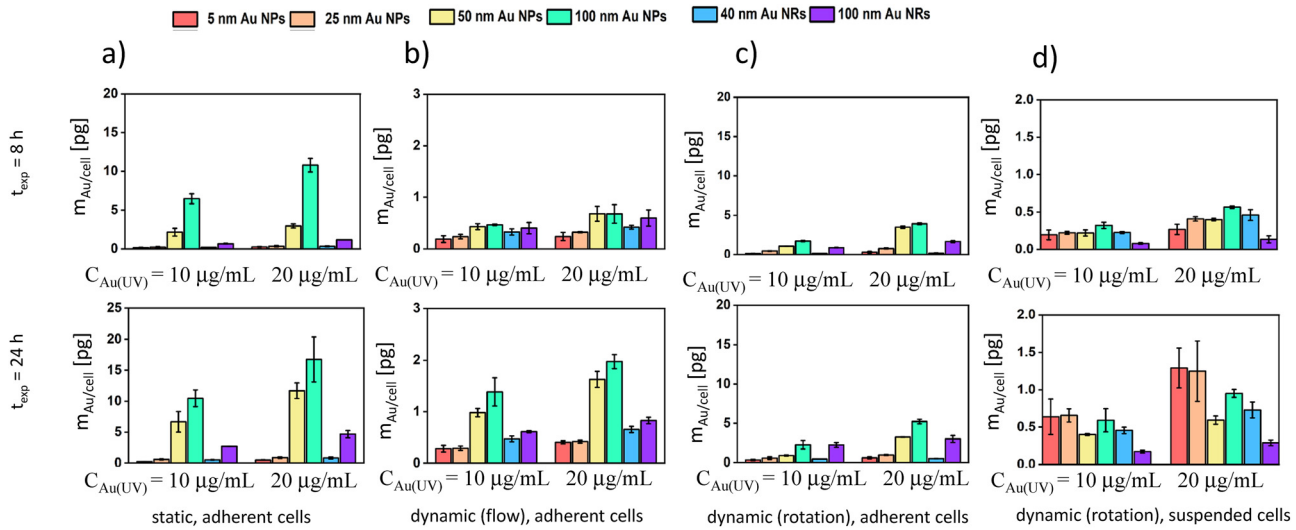

Fig. 2 Amount of Au NPs $m_{Au/cell}$, which have been internalized per cell after exposure for time t_{exp} in volume V_{exp} = 6 mL of serum-containing medium with added NPs at concentration $C_{Au(UV)}$, under the 4 different exposure geometries shown in Fig. 1. This figure is a compilation of the figures for the whole data set, as given in the SI.

of the exposure medium (V_{epx}; see Fig. SIV-1, SIV-3 and SIV-9). For this reason, the following discussion will be limited to only 2 of the 3 measured time points (t_{exp} = 8 h, 24 h), with exposure volume V_{exp} = 6 mL. The data are shown in Fig. 2, and as detailed above, are representative of the full data set provided in the SI.

Quantification of the maximum amount of internalized Au dependent on the exposure geometry

For all NP sizes, the number of endocytosed NPs depends strongly on the exposure geometry. The actual biological process of endocytosis starts once NPs come into contact with the cell membrane. Endocytosis itself is here considered as a first approximation to be independent of exposure geometry, as the entire study has been carried out with the same cell type in the same culture medium. However, before endocytosis may start, the NPs need to reach the surface of the cell, which in cell culture experiments is governed by physicochemical processes, such as diffusion and sedimentation.[19,20] After reaching the cells, the NPs need to adhere to the cell membrane for a sufficient time so that they can be endocytosed.

With a simplified model, one can imagine that the adherence of NPs to the cell surface is different for adherent and suspended cells. While adherent cells are stretched and flat on the cell culture substrate to maximize contact, suspended cells are rather rounded and avoid adherence to cell culture substrates. Therefore, NPs should also "stick" better to adherent cells than to suspended cells. This corresponds to the result in the case of suspended cells, where NP uptake was found to be lower than in the case of the 3 different exposure geometries based on adherent cells (Fig. 2d *versus* Fig. 2a–c). The difference in the "sticking" of NPs to the cell membrane between adherent and suspended cells is a biological effect. The following section discusses the physicochemical factors that influence the transport of NPs to the cell surface.

As mentioned, for NPs reaching cells, apart from diffusion, sedimentation is also important.[19,20] From the 3 exposure geometries with adherent cells, the one with the dynamic flow conditions, in which NPs are pumped in a flow channel above the cells, shows the lowest NP uptake by cells (Fig. 2b *versus* Fig. 2a and c). In the flow channel, the effects of sedimentation are overruled by "mixing". We note that, even when the medium flow above the cells is not turbulent, the NPs are taken by the pump from a reservoir under continuous mixing, where the NPs are well dispersed, and the time the NPs reside in the flow channel is not sufficient for sedimentation. Direct comparison is complicated because cells were seeded at a density of 40 000 cells cm^{-2} under dynamic flow, whereas the seeding density for the static and rotated cultures was 24 000 cells cm^{-2}. This was done as the cross-sectional area of the adherent cells in the fluid channel was found to be smaller than those of the cells under static/rotation conditions. With the chosen conditions, the coverage of the surface by cells was comparable. According to Fig. SII-3, the proliferation rate of all adherent cell cultures was similar, and at the time of seeding, cells had not yet formed a fully confluent layer. For this reason, we hypothesize that the conditions can be compared, although a absolute direct comparison between the uptake under both conditions has to be interpreted with caution.

There may be greater uptake of NPs in the rotation cell culture flask (Fig. 2c *versus* Fig. 2b), whereby the above mentioned differences need to be considered, *i.e.* smaller cells in the case of the fluid channel. The rotation speed is relatively low (10 rpm) and thus there may be sedimentation effects. To visualize this, one may think of a bottle filled with sand, which is rotated around the long axis of the bottle: the sand will predominantly remain at the bottom due to sedimentation, despite the rotation. In the static cell culture, there is no mixing of the NPs apart from thermal diffusion, and thus sedimentation is paramount for the bigger NPs, resulting in the highest uptake of NPs (Fig. 2a *versus* Fig. 2b and c).

For both the adherent rotated cells (Fig. 2c) and the rotated suspended cells (Fig. 2d), the culture substrates/tubes are rotated at the same speed (10 rpm). One might argue that, as the surface of the culture flask facing downward is larger for the adherent cells (Fig. 2c) than the corresponding surface of the culture tube facing downward, (Fig. 2d; see Fig. SII-1 for a comparison of the geometries), the relative rcf ($\times g$) is higher in the flasks (Fig. 2c) than for the tube (Fig. 2d), making the effect of sedimentation more important for the geometry of cells shown in Fig. 2c compared to the geometry of cells shown in Fig. 2d. Whether this effect influences the higher uptake in Fig. 2c *versus* Fig. 2d can only be speculation with the available data set. On the other hand, the reduced NP adhesion to suspended cells (Fig. 2d) *versus* adherent cells (Fig. 2c) seems plausible for explaining why the overall NP uptake for the rotating suspended cells is lowest.

The data show that the maximum amount of internalized Au NPs (in terms of intracellular Au) varies by up to one order of magnitude for different exposure geometries, having the highest uptake for a static culture of adherent cells, followed by slowly rotated adherent cells and then by adherent cells in a flow channel, with the lowest uptake for rotated cell suspensions. Notably, which of the different NP types leads to the maximum uptake may be different for the different exposure geometries and will be discussed in the following section.

Size dependence of the quantity of internalized Au in the dependence of the exposure geometry

The data shown in Fig. 2 show that the biggest effect of NP size on their uptake is present for adherent cells in static culture (Fig. 2a). This has been suggested to be due to sedimentation of the bigger NPs, ''falling down'' on the cells, meaning many of the NPs touch the cell membrane, where they can be endocytosed, in line with previous studies.[19,20] Note that the volume of the 100 nm long NRs is smaller than the volume of 100 nm diameter spheres, and due to their smaller mass, they sediment less.[21] A similar size dependence can also be seen for adherent cells, where the cell culture substrate is slowly rotated. Where mixing of the NPs in the medium upon rotation is not predominant, there will still be an accumulation of NPs at the bottom, and thus, when the cell flask is oriented in such a way that the side where the cells are adherent is at the bottom, the bigger NPs accumulate more due to sedimentation and thus are more internalized. When the cell flask is oriented in such a way that the side where the cells are adherent is at the top, there is no uptake, as the medium with the NPs is not in contact with the cells (the flask is not completely filled). Thus, on average, the size-dependent effect of sedimentation is to favor the uptake of bigger NPs. However, this effect is reduced as the effect is modulated upon rotation of the flask (Fig. 2c *versus* Fig. 2a).

For the adherent cells with medium flowing above the cells in a flow channel, there is only slightly enhanced uptake of bigger NPs (Fig. 2b). As mentioned, the NP stock solution is mixed to ensure a homogeneous distribution of NPs in the medium, minimizing sedimentation as the NPs in the medium pass over the cells.

The size dependence for NP uptake is completely different for cells in suspension (Fig. 2d *versus* Fig. 2a–c). Notably, there is also a different time dependence, showing a slower uptake (24 h *versus* 8 h) than for the adherent cells, which could be understood by assuming that the NPs ''stick'' less to the cells. In the case of suspended cells, the data from Fig. 2d show that the highest amount of intracellular Au is found for the smallest NPs. This effect might be related to the actual biological process of endocytosis; although there are interesting experimental and computational approaches trying to unravel the size dependence of membrane wrapping around NPs,[31–35] none of these studies completely fits our results.

Limits of the direct comparison of the different exposure geometries and NP sizes

Ideally, for a direct comparison, only one parameter should be varied, while all others are kept constant. Obviously, in the study presented here, this was not fully achievable, and thus possible errors need to be discussed. Concerning the NPs, there is already some uncertainty in their concentration, as different methods for determining their concentration do not provide identical results (*i.e.* ICP–MS *versus* UV/vis data). In the worst case, this was the difference between 2.8×10^5 μg L^{-1} and 5.5×10^5 μg L^{-1} (100 nm Au NRs, Table SI-1), corresponding to an uncertainty of (5.5–2.8)/5.5 $\approx$ 50%. Also, while all NPs were coated with the same type of polymer, apart from the intended differences in size, there are also variations in the zeta potential; see Table 1. All NPs were highly negatively charged; thus, there is no strong influence expected from the variation in their zeta potential on the uptake by cells. In the worst-case scenario, the maximum difference between the zeta potentials of the 5 nm Au NPs (−31.8 mV, see Table 1) and the 100 nm Au NPs (−47.1 mV), corresponds to a variation of (47.1–31.8)/47.1 $\approx$ 30%. Uptake of NPs by cells will certainly not depend linearly on their physicochemical properties. But, even assuming this, uncertainties in concentration determination and variations in zeta potentials cannot explain the large differences in their cellular uptake, as presented in Fig. 2, which can be an order of magnitude higher.

Concerning the cells, additional limitations need to be discussed. Changing the cell culture conditions also affects the cells themselves, such as the proliferation rate (*cf.* Fig. SII-3). It is important that uptake experiments were carried out under conditions where no significant reduction in cell viability was observed (Fig. SIII-1 to Fig. SIII-4). HeLa cells are adherent cells, and to use them as suspended cells, mechanical manipulation—rotating the substrate below them—was required to prevent attachment. This is naturally a limitation. Either the same type of cells can be compared, meaning that one has to force cells not to adhere to warrant for suspended cells, or an adherent cell line is compared with a suspended cell line, involving the comparison of two different cell types. Also, as discussed above, the different geometries, *e.g.* static *versus* rotation culture, will not have exactly the same exposure area. This clearly tells us that the results of this study have a semi-quantitative character, which, however, for the above mentioned problems would be hard to avoid.

Conclusions

An important goal of studying the basic interaction of nanoparticles and cells is to relate the physicochemical properties of nanoparticles to their biological activity, such as how they are internalized by cells. Based on this, how NPs would ''behave'' *in vivo* could be predicted. This would help to tune the properties of NP-based nanomedicines towards their desired biological action. Many attempts have been made in this direction,[36–45] but a comprehensive prediction has not yet been achieved.

Apart from the overwhelming complexity of such an approach, fundamental problems are involved. One is that most physicochemical parameters are entangled, and their effects cannot be analyzed separately.[36] The other problem, as can be seen in this work, is the choice of appropriate cell culture geometries. As shown in Fig. 2a–c *versus* Fig. 2d, a change in exposure geometry can change from the favorable uptake of bigger NPs to the favorable uptake of smaller NPs. Interpretation of *in vitro* results from cell culture models, thus always has to be done with utmost care. The finding that in adherent static cell cultures, the uptake of bigger NPs is enhanced due to sedimentation effects may not be relevant for *in vivo* scenarios. Unfortunately, there may not be one ''best'' *in vitro* culture geometry, and cell culture conditions may need to be optimized for relevance in different *in vivo* scenarios. Culture of adherent cells in a flow channel might, for example, be useful for predicting NP uptake by cells in the walls of blood vessels, like endothelial cells. Cell suspensions might be more appropriate to investigate NP uptake by cells in blood, like macrophages.

However, one should not misinterpret these conclusions to say that *in vitro* cell culture systems are ''useless'' simply because they cannot fully replicate the *in vivo* environment. As pointed out in the introduction, due to the possibility of upscaling *in vitro* measurements to sample sizes, which cannot be achieved with *in vivo* measurements, there is an argument in favor of conducting such studies. The conclusion rather, should be that limitations of *in vitro* cell systems need to be understood and respected. Optimization of the *in vitro* culture geometry should be undertaken for the different routes of *in vivo* scenarios, bringing them as close as possible to the ''real'' environment.

Author contributions

Nanoparticle synthesis and characterization: YH, XS, YK; ICP-MS analysis: YL, BQ; set up of flow channel and rotated cell culture: SYVS, YW; cell culture, viability and uptake studies: YH, ZL; data analysis: YH, MF; supervision and concept development: CG, WJP, NF; writing of first draft: YH, MF, WJP; all authors read, improved, and approved the final manuscript.

Conflicts of interest

The authors declare that they having no conflict of interest.

Data availability

All data are provided in the supplementry information (SI), in particular the ones which have been used to generate graphs and tables. Supplementry information: contains (i) Details about the synthesis and characterization of gold nanoparticles, (ii) Details of the cell culture and exposure geometries, (iii) Cell viability data, and (iv) Details concerning the cellular uptake of NPs and NRs. See DOI: https://doi.org/10.1039/d5nh00621j.

Acknowledgements

WJP and NF are grateful to Prof. Dr Mark Illies and Dr Wendel Wohlleben for helpful discussions at the beginning of this project. This project was supported by the DFG (SFB 1700 – Immunregulation in der Leber: von Homöostase zur Erkrankung, grant NF). YH, XS, MF, ZL, YL, BQ, and YK are grateful to China Scholarship Council (CSC) for PhD fellowships. WJP acknowledges funding by the Hamburgische Landesforschungsförderung ''Transiente CAR-Effektorzellen: neue Ansätze zu ihrer Herstellung und effizienten Anwendung (transCAR)''. CG is funded by the DFG (priority program 2416 CodeChi GO 2528/10-1 and GO 2528/9-1). YW is supported by the Mildred Scheel Cancer Career Center HaTriCS4 at University Medical Center Hamburg-Eppendorf.

References

1 N. Feliu and W. J. Parak, Developing future nanomedicines, *Science*, 2024, **384**(6694), 385–386.
2 C. Jubelin, *et al.*, Three-dimensional in vitro culture models in oncology research, *Cell Biosci.*, 2022, **12**(1), 155.
3 T. S. Biju, V. V. Priya and A. P. Francis, Role of three-dimensional cell culture in therapeutics and diagnostics: an updated review, *Drug Delivery Transl. Res.*, 2023, **13**(9), 2239–2253.
4 S. M. Badr-Eldin, *et al.*, Three-dimensional in vitro cell culture models for efficient drug discovery: Progress so far and future prospects, *Pharmaceuticals*, 2022, **15**(8), 926.
5 G. Rauner, P. B. Gupta and C. Kuperwasser, From 2D to 3D and beyond: the evolution and impact of in vitro tumor models in cancer research, *Nat. Methods*, 2025, 1–12.
6 C. J. Ramírez-Flores, *et al.*, Transcending dimensions in apicomplexan research: from two-dimensional to three-dimensional in vitro cultures, *Microbiol. Mol. Biol. Rev.*, 2022, **86**(2), e00025-22.
7 L. Kim, *et al.*, A practical guide to microfluidic perfusion culture of adherent mammalian cells, *Lab Chip*, 2007, **7**(6), 681–694.
8 E. W. Young and D. J. Beebe, Fundamentals of microfluidic cell culture in controlled microenvironments, *Chem. Soc. Rev.*, 2010, **39**(3), 1036–1048.
9 H. Wang, *et al.*, 3D cell culture models: Drug pharmacokinetics, safety assessment, and regulatory consideration, *Clin. Transl. Sci.*, 2021, **14**(5), 1659–1680.

10 D. L. Hughes, *et al.*, Dynamic physiological culture of ex vivo human tissue: a systematic review, *Cancers*, 2021, **13**(12), 2870.
11 S. Salatin, S. M. Dizaj and A. Y. Khosroushahi, Effect of the surface modification, size, and shape on cellular uptake of nanoparticles, *Cell Biol. Int.*, 2015, **39**(8), 881–890.
12 P. Sabourian, *et al.*, Effect of physico-chemical properties of nanoparticles on their intracellular uptake, *Int. J. Mol. Sci.*, 2020, **21**(21), 8019.
13 Y. Liu, *et al.*, Programmed drug delivery system based on optimized "size decrease and hydrophilicity/hydrophobicity transformation" for enhanced hepatocellular carcinoma therapy of doxorubicin, *Nanomedicine*, 2018, **14**(4), 1111–1122.
14 D. Chen, *et al.*, Promoting inter-/intra-cellular process of nanomedicine through its physicochemical properties optimization, *Curr. Drug Metab.*, 2018, **19**(1), 75–82.
15 E. C. Cho, Q. Zhang and Y. N. Xia, The effect of sedimentation and diffusion on cellular uptake of gold nanoparticles, *Nat. Nanotechnol.*, 2011, **6**(6), 385–391.
16 J. Han, *et al.*, Acute and chronic shear stress differently regulate endothelial internalization of nanocarriers targeted to platelet-endothelial cell adhesion molecule-1, *ACS Nano*, 2012, **6**(10), 8824–8836.
17 T. G. Hammond, *et al.*, Cell spinpods are a simple inexpensive suspension culture device to deliver fluid shear stress to renal proximal tubular cells, *Sci. Rep.*, 2021, **11**(1), 21296.
18 L. Beresova, *et al.*, Uncovering pre-cytokinetic block in cancer cells under shear stress using a disturbed flow-generating device, *Sci. Rep.*, 2025, **15**(1), 6457.
19 N. Feliu, *et al.*, Quantitative Particle–Cell Interaction: Some Basic Physicochemical Pitfalls, *Langmuir*, 2017, **33**, 6639–6646.
20 N. Feliu, *et al.*, Correction to "Quantitative Particle−Cell Interaction: Some Basic Physicochemical Pitfalls", *Langmuir*, 2017, **40**, 8291.
21 X. Sun, *et al.*, Tracking stem cells and macrophages with gold and iron oxide nanoparticles – The choice of the best suited particles, *Appl. Mater. Today*, 2019, **15**, 267–279.
22 J. Hühn, *et al.*, Selected Standard Protocols for the Synthesis, Phase Transfer, and Characterization of Inorganic Colloidal Nanoparticles, *Chem. Mater.*, 2017, **29**, 399–461.
23 W. Haiss, *et al.*, Determination of Size and Concentration of Gold Nanoparticles from UV-Vis Spectra, *Anal. Chem.*, 2007, **79**(11), 4215–4221.
24 N. Feliu, *et al.*, Nanoparticle dosage-a nontrivial task of utmost importance for quantitative nanosafety research, *Wiley Interdiscip. Rev.: Nanomed. Nanobiotechnol.*, 2016, **8**, 479–492.
25 P. del_Pino, *et al.*, Basic Physicochemical Properties of Polyethylene Glycol Coated Gold Nanoparticles that Determine Their Interaction with Cells, *Angew. Chem., Int. Ed.*, 2016, **55**, 5483–5487.
26 R. A. Sperling, *et al.*, Size Determination of (Bio-) Conjugated Water-Soluble Colloidal Nanoparticles: A Comparison of Different Techniques, *J. Phys. Chem. C*, 2007, **111**(31), 11552–11559.
27 G. B. Braun, *et al.*, Etchable plasmonic nanoparticle probes to image and quantify cellular internalization, *Nat. Mater.*, 2014, **13**(9), 904–911.
28 S. Hou, *et al.*, Quantitative Differentiation of Cell Surface-Bound and Internalized Cationic Gold Nanoparticles Using Mass Spectrometry, *ACS Nano*, 2016, **10**(7), 6731–6736.
29 M. Semmling, *et al.*, A Novel Flow-Cytometry-based Assay for Cellular Uptake Studies of Polyelectrolyte Microcapsules, *Small*, 2008, **4**(10), 1763–1768.
30 M. Feng, *et al.*, Quantification of optimizing cellular uptake and excretion of nanoparticles by aggregation and de-aggregation mediated size changes, *Nano Today*, 2025, **65**, 102819.
31 A. H. Bahrami, *et al.*, Wrapping of nanoparticles by membranes, *Adv. Colloid Interface Sci.*, 2014, **208**, 214–224.
32 Y. Li, *et al.*, Selective membrane wrapping on differently sized nanoparticles regulated by clathrin assembly: A computational model, *Colloids Surf., B*, 2022, **214**, 112467.
33 S. L. Zhang, *et al.*, Size-Dependent Endocytosis of Nanoparticles, *Adv. Mater.*, 2009, **21**(4), 419–424.
34 X. Meng and X. Li, Size Limit and Energy Analysis of Nanoparticles during Wrapping Process by Membrane, *Nanomaterials*, 2018, **8**, 899.
35 C. Contini, *et al.*, Size dependency of gold nanoparticles interacting with model membranes, *Commun. Chem.*, 2020, **3**, 130.
36 M. Xu, *et al.*, How Entanglement of Different Physicochemical Properties Complicates the Prediction of in Vitro and in Vivo Interactions of Gold Nanoparticles, *ACS Nano*, 2018, **12**, 10104–10113.
37 S.-L. Song, *et al.*, Complex in vitro 3D models of digestive system tumors to advance precision medicine and drug testing: Progress, challenges, and trends, *Pharmacol. Ther.*, 2022, **239**, 108276.
38 O. Urzì, *et al.*, Three-dimensional cell cultures: the bridge between in vitro and in vivo models, *Int. J. Mol. Sci.*, 2023, **24**(15), 12046.
39 L. N. Nguyen, *et al.*, The mechanisms of nanoparticle delivery to solid tumours. Nature Reviews, *Bioengineering*, 2024, **2**(3), 201–213.
40 J. L. Wu, *et al.*, The pathways for nanoparticle transport across tumour endothelium, *Nat. Nanotechnol.*, 2025, 1–11.
41 S. K. Hobbs, *et al.*, Regulation of transport pathways in tumor vessels: role of tumor type and microenvironment, *Proc. Natl. Acad. Sci. U. S. A.*, 1998, **95**(8), 4607–4612.
42 L. N. Nguyen, *et al.*, The exit of nanoparticles from solid tumours, *Nat. Mater.*, 2023, **22**(10), 1261–1272.
43 K. Y. Fung, G. D. Fairn and W. L. Lee, Transcellular vesicular transport in epithelial and endothelial cells: Challenges and opportunities, *Traffic*, 2018, **19**(1), 5–18.
44 Z. P. Lin, *et al.*, Macrophages actively transport nanoparticles in tumors after extravasation, *ACS Nano*, 2022, **16**(4), 6080–6092.
45 V. P. Chauhan, *et al.*, Normalization of tumour blood vessels improves the delivery of nanomedicines in a size-dependent manner, *Nano-Enabled Medical Applications*, Jenny Stanford Publishing, 2020, pp. 279–311.